SCHOOL OF MECHANICAL ENGINEERING

UNIVERSITY OF LEEDS

MECH3890 – Individual Engineering Project

PROJECT TITLE: Numerical Investigation into the Performance of a Supersonic Busemann Biplane for Different Off-design Conditions

PRESENTED BY	César Sánchez Aguado
SUPERVISED BY	Natalie Gilkeson

If the project is industrially linked, tick this box and provide details below ☐

COMPANY NAME AND ADDRESS:

N/A

STUDENT DECLARATION (from the "LU Declaration of Academic Integrity")

I am aware that the University defines plagiarism as presenting someone else's work, in whole or in part, as your own. Work means any intellectual output, and typically includes text, data, images, sound or performance. I promise that in the attached submission I have not presented anyone else's work, in whole or in part, as my own and I have not colluded with others in the preparation of this work. Where I have taken advantage of the work of others, I have given full acknowledgement. I have not resubmitted my own work or part thereof without specific written permission to do so from the University staff concerned when any of this work has been or is being submitted for marks or credits even if in a different module or for a different qualification or completed prior to entry to the University. I have read and understood the University's published rules on plagiarism and also any more detailed rules specified at School or module level. I know that if I commit plagiarism I can be expelled from the University and that it is my responsibility to be aware of the University's regulations on plagiarism and their importance. I re-confirm my consent to the University copying and distributing any or all of my work in any form and using third parties (who may be based outside the EU/EEA) to monitor breaches of regulations, to verify whether my work contains plagiarised material, and for quality assurance purposes. I confirm that I have declared all mitigating circumstances that may be relevant to the assessment of this piece of work and that I wish to have taken into account. I am aware of the University's policy on mitigation and the School's procedures for the submission of statements and evidence of mitigation. I am aware of the penalties imposed for the late submission of coursework.

Date: 4/05/2023
Signed

Abstract

Due to the failure of supersonic transport, Busemann biplanes are being investigated to assess their viability. A CFD case was developed to study the influence of Mach number and AoA in the performance of a Busemann biplane. Since the aerofoil presents great inefficiencies in off-design conditions, two parametric studies are performed for a range of Mach from 1.7 to 2.1 and AoA from 0 to 3. The SA turbulence model provided the most accurate results compared to numerical validation, which permitted analysing of aerodynamic coefficients, C_p and the shock wave pattern.

After studying the drag and lift coefficients, the results suggest that a significant reduction in the wave drag can be accomplished in velocity design conditions, whereas the drag is increased in the off-design conditions. On the contrary, the AoA study provides insight into the increase in aerodynamic efficiency, which is linearly proportional to the AoA.

Contents

Nomenclature

Symbol	Definition	Unit
AoA	Angle of Attack	$^\circ$
c	Chord of the biplane	m
C_d	Total drag coefficient	-
$C_{d,f}$	Friction drag coefficient	-
$C_{d,p}$	Pressure drag coefficient	-
C_l	Total lift coefficient	-
C_p	Pressure coefficient	-
CFD	Computational Fluid Dynamics	-
FVM	Finite Volume Method	-
GCI	Grid Convergence Index	-
Re	Reynolds number	-
y^+	Non-dimensional wall-adjacent grid height	-
ϵ	Error	-

List of Figures

List of Tables

1 Introduction

1.1 Introduction

The development of supersonic aircraft has been a topic of great interest in the aerospace industry for several decades. However, economic and environmental sustainability is yet to be achieved by commercial aircraft, which are prevented from supersonic speeds because of shock waves and the complexity that high-speed entails.

Even though several scientific developments in the fields of materials and propulsion promoted the appearance of supersonic aeroplanes, few advances have been made in the framework of commercial aviation, with sporadic unsuccessful attempts like the Concorde (1969-2003). The reason is supersonic flight's low efficiency: it requires significant amounts of fuel because of the creation of shock waves and their associated drag. Furthermore, sonic booms introduce turbulence, noise, and temperature problems that also difficult the production of profitable supersonic aircraft. The future of aviation can accomplish supersonic transport as a renewed effort is made to design sustainable aircraft (National Research Council, 1997).

To reduce the fuel costs of supersonic flight, it is key that future aircraft reduce their drag, mainly associated with shock waves. In that sense, many alternatives have been proposed to increase the efficiency of supersonic aircraft, optimising the fuselage and the wing. This study focuses on the drag study of a 2D of a Busemann biplane, a supersonic aerodynamic profile proposed by Adolf Busemann in 1935 (Busemann, 1935). It is based on the same principles as the diamond aerofoil used in military applications, although its better performance in design conditions makes it suitable for commercial purposes. The Busemann biplane is formed by two isosceles triangles opposing each other, as seen in Figure 1, whose main parameters will depend on the design conditions desired. This concept aims to reduce the wave drag contribution associated with shock waves using the wave-cancellation effect.

To gain insight into the viability of the biplane in design and off-design conditions, this project uses CFD to study the viability of a Busemann biplane, explaining all the steps necessary to carry out the simulations. CFD is a powerful tool that allows engineers to determine a plane's behaviour under many flow regimes, using numerical solution methods to analyse a case quickly. It is particularly important in the analysis of supersonic flows due to the difficulties and

costs of experimental procedures. As a previous step to experimental testing, computational analyses usually use the FVM, a discretisation technique that divides the system into smaller volumes. Then, several flow assumptions can be made to obtain a solution in the finite elements for the governing equations. This allowed determining multiple variables in many locations in the system, using cost and time-efficient methods. The CFD process will be done with Ansys Fluent 2021 R1, a CFD software that includes a Workbench's Geometry and Mesh tools to set up the simulations.

Although it could not be implemented in actual aircraft, many modern studies base their designs on the Busemann biplane. This report aims to understand the physics of the aerofoil as well as the main features of the flow around it. Its benefits and drawbacks will be assessed in terms of aerodynamic coefficients and efficiency, emphasising the analysis of the shock wave pattern.

1.2 Aim

The aim of this project is to assess the performance of a 2D Busemann biplane under design and off-design supersonic flow conditions, studying through CFD the drag, lift and shock wave patterns over a range of Mach numbers and AoA.

1.3 Objectives

- Study different configurations of Busemann biplanes, creating a suitable 2D model in Ansys Workbench's Geometry.
- Set up of the simulation, based on the literature review, implementing the right boundary conditions, turbulent model and general set-up.
- Build a mesh with the proper refinements to capture the flow features, focusing on the flow around the biplane and the shockwaves, performing a grid independence study for design conditions.
- Simulate the case for different Mach numbers and AoA for design and off-design conditions. Validate the results with the literature.
- Obtain conclusions about the results and relate them with supersonic transport aircraft design. Assess how the Mach number and AoA affect the drag and lift. Determine if there is a speed at which the airflow starts to be choked and the impact of that behaviour in the drag.

- Evaluate the different patterns of the shock waves and how the biplane design affects the reflection and expansion waves.

1.4 Report layout

- Section 2 will cover the theoretical background needed to understand the physics of the Busemann biplane and assess the analysis of the results of the simulations.
- Section 3 covers the explanation of the model in design conditions, which will be applied to all the simulations carried out throughout the report. This section is organized so that the workflow of a CFD study can be followed. The model is then validated by comparing results with the literature.
- Section 4 provides the results of the velocity and AoA parametric studies, comparing the results of those of Section 3. Key findings are discussed and related with the performance of a Busemann biplane.
- Section 5 summarizes the achievements and conclusions of the project. Future work is included to expand the knowledge of drag reductions of supersonic biplanes.

2 Theoretical Background

2.1 Physics of the flow

In supersonic flows, the speed of the stream is greater than the local speed of sound, which compresses the fluid molecules and reduces the flow area, causing a shock wave (NASA, 2021). Shock waves are regions in the fluid in which the gradients of the flow properties are discontinuous (Anderson, 2003). For small-angled wedges and high speeds like Busemann aerofoil, an oblique shock is generated, usually creating a weak shock that does not reduce the Mach number of the stream to subsonic levels (NASA, 2021). Shock waves greatly impact the total drag contribution of a supersonic aircraft, which is decomposed into wave and viscous drag. According to Emanuel (2001), wave drag is more critical for high Mach numbers due to the more significant pressure difference in the flow before and after the flow. Busemann biplanes are designed to eliminate this drag so that more efficient aircraft are developed.

Busemann biplanes are characterised by the interference between shock waves inside their shape. This scenario gives rise to complex wave patterns whose impact could cause great pressure and heat transfer loads capable of damaging the surface of the biplane (Délery, 1999). When two shocks coalesce, they form several shocks and weak shocks or expansion fans separated by a slip surface (NASA, 2021). Busemann biplanes use this interaction to eliminate the drag associated with their thickness (Kusunose, 2011): for design conditions, the strong shock wave generated at the leading edge will exactly reach the inner corner point of the opposite airfoil and will be cancelled by the expansion wave at that point (Hu et al., 2011). The wave-cancellation phenomenon occurs in design conditions where the inlet and outlet pressure are the same, having a theoretical wave drag of zero (Zhai et al., 2020), as seen in Figure 1 (Matsushima, 2006). In reality, the entropy generated by the shocks increases the wave drag, although it is still relatively low. Even so, Busemann biplanes present a characteristic low drag and low sonic boom compared to a classical double-wedged supersonic aerofoil.

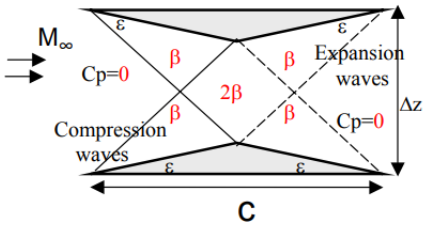

Figure 1: Busemann biplane operating at ideal conditions

Despite its advantages, Busemann biplanes show several problems in off-

design conditions (flow choking and hysteresis), which is why it is important to assess their performance when the speed and AoA deviate from design conditions. The internal contraction section causes the choking of the flow (Liu et al., 2019), increasing the wave drag and the complexity of starting the biplane (Zhai et al., 2020). Yamashita (2013) states that going from a 2D to a 3D case reduces the choking problem due to the three-dimensional effect, introducing, however, vorticity effects near the wing tips and increasing the induced drag. On the other hand, the hysteresis problem causes a higher drag when the airfoil is accelerating, thus presenting different behaviours for the same flow conditions.

2.2 State of the art

Several authors have studied designs that improve the performance of Busemann biplanes in off-design conditions. To overcome the choking problem by increasing the ratio between the throat and inlet areas. Yamashita (2007) employs flaps at both the leading and trailing edges of the biplane to change these section areas. Other approaches include staggered airfoil configurations that maximise the throat area in exchange for slightly losing efficiency because of wave-cancellation (Patidar et al., 2016). Patidar justifies stagger due to its vast improvement in performance in the subsonic region.

Zhai (2020) combines the geometries of the Busemann and Licher biplanes to create an asymmetric design with a triangular lower surface and an upper flat plate. Maintaining the wave-cancellation properties of the Busemann biplane, this new design not only reduces the choking of the flow in off-design conditions, thus obtaining a biplane that is easier to start than the original model, but it also has a lower drag and higher lift-to-drag ratio.

Kusunose (2010) describes that the choking of the flow would involve hysteresis problems during the acceleration stage, increasing the drag of the biplane even for design conditions when the velocity is being increased. His research reveals that maximising the throat-to-inlet area ratio would reduce this problem, a solution in concordance with previous solutions to minimise choked flow.

3 Aerofoil in Design Conditions

3.1 Introduction

In this chapter, the Busemann biplane will be studied under ideal conditions. For the design selected, ideal conditions consist of a Mach number of 1.7 at zero lift (zero AoA). The biplane's drag reaches a minimum in that condition because the shock waves favour the wave-cancellation effect. This section explains the modelling process and set-up of the simulations, which will be maintained for future analyses. The order in which topics are presented tends to follow a chronological order so that the process is easily followed. After researching this case, the data will be validated, serving as a comparison for off-design conditions.

3.2 Methodology

3.2.1 Biplane geometry

The geometry selection is the first step of the modelling process of a CFD simulation (NASA, 2021). Its importance relies on the fact that this is the shape that will be analysed, serving as an input for the grid generation. Therefore, its design considers the meshing strategy discussed later. Complex geometries may cause high computation costs and divergence of the results, but no further simplifications are needed due to the supersonic biplane's simplicity. The main factor that has been taken into account in choosing the design of the aerofoil is the availability of validation data (Kusunose et al., 2011, and Patidar et al., 2016). Of course, this impacts the Mach number of the ideal conditions and how shock waves are developed in the domain. The Busemann biplane is seen in Figure 2, where z/c=0.5, t/c=0.05 and c=1 m.

3.2.2 Domain geometry

The domain was selected so that its boundary conditions do not interfere with the behaviour of the flow. Since the size of the external domain needed changes for every Mach number, it has to be ensured that this is satisfied for all the cases analysed. On the other hand, excessively large domains increase the number of cells and decrease computational efficiency.

Zhai et al. (2020) and Ma et al. (2020) use a rectangular domain, which facil-

itates the generation of a structured mesh because of the shape of the biplane. Whereas supersonic speeds require few cells upstream of the aerofoil, the size of the downstream domain is critical. Similar studies present a control volume with 20 to 50 chords downstream of the airfoil (Hosseini (2019) and Le et al. (2015), respectively). A sensible domain of 50 chords was selected, as seen in Figure 2. The domain was then divided into sectors to allow higher control in the meshing process.

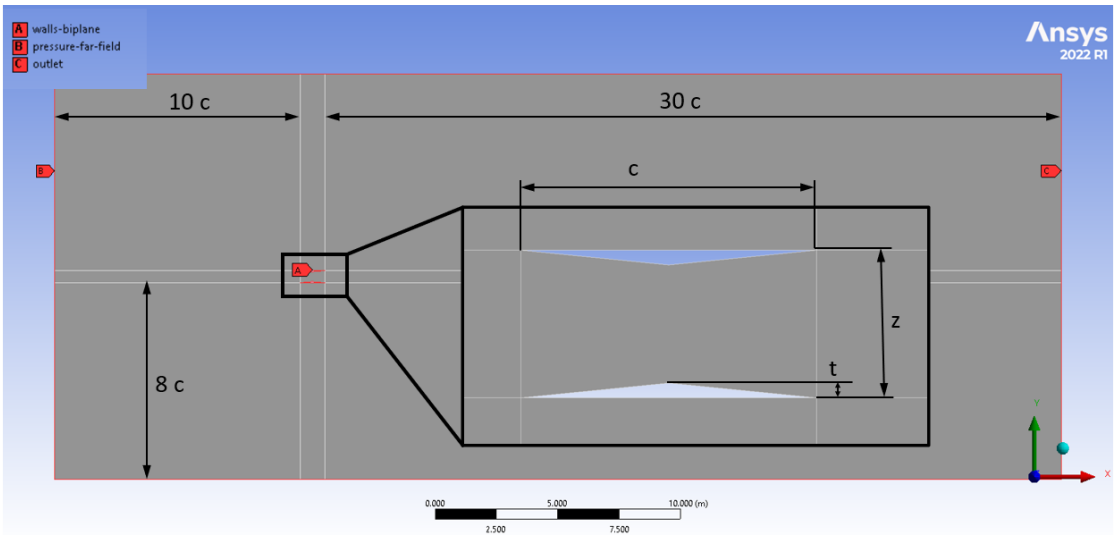

Figure 2: Visual appearance of the solution domain

3.2.3 Meshing

The domain's geometry makes it suitable to implement a structured grid, characterised by quadrilateral cells and high quality. Structured meshes require less memory than unstructured ones (Bern and Plassmann, 2000) and are less susceptible to numerical diffusion. While having the drawback of being difficult to create in complex geometries, a structured mesh is chosen for the aerofoil because of its lower computational cost and better results.

The philosophy followed is to cluster the cells in the areas of the domain in which the gradients of the flow are more significant, that is, around the walls of the biplane and between them, where the shock waves will appear. This is controlled by setting the number of divisions and the growth rate of the edges created in the domain geometry, allowing a smooth transition between the bigger outer cells and those around the biplane and between the different sections of the domain. The growth rate is chosen so that $y^+ \approx 1$ after refinements (explained in the selection of the turbulent model), which allows capturing the high gradients of the boundary layer.

Before carrying on with the simulations, the mesh quality was checked by analysing the parameters of the cells. The maximum skewness in the mesh was 0.0635, indicating almost ideal orthogonal cells (SimScale, 2022). In the region of interest, the aspect ratio of the cells was close to 1, overall presenting a good element quality. Then, the meshes were simulated to make adaptions in the velocity or pressure high-gradient cells to capture the shock waves, as seen in Figure 3. The refinements consist of dividing existing cells into smaller cells, reducing their size by two in each direction and increasing the mesh density on the regions of interest. This process was performed twice (displayed in Figure 4); thus, the initial meshes were designed with a $y^+ \approx 4$ for the final ones to have the desired $y^+ \approx 1$. These simulations present the set-up explained in the following section but were made before the turbulence model analysis. Therefore, for the independence grid analysis, the SA model (Spalart and Allmaras, 1992) was selected based on the articles by Kusunose et al. (2011), Patidar et al. (2016) and Maruyama et al. (2011).

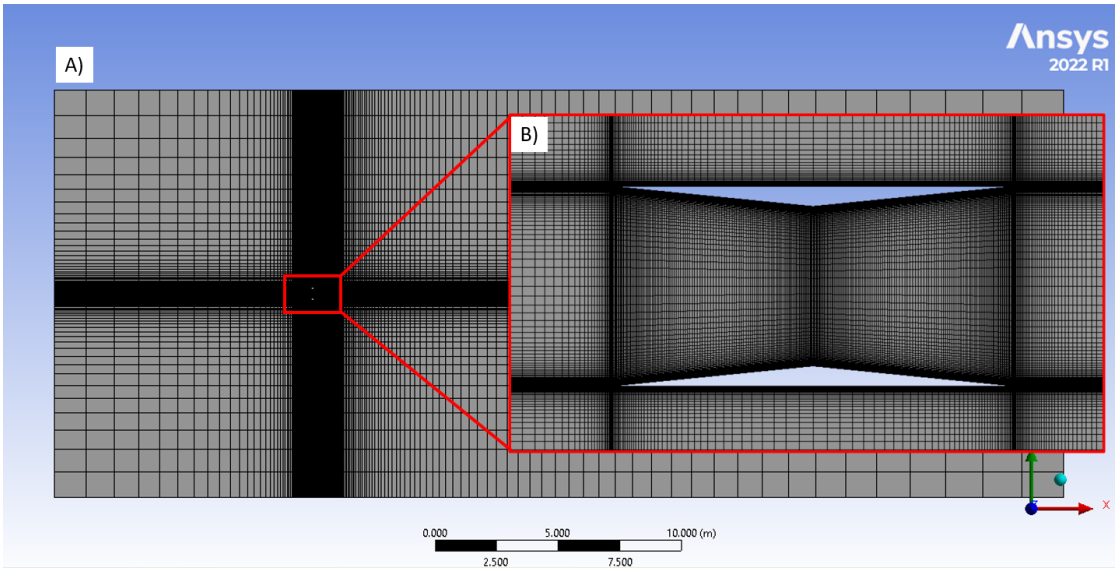

Figure 3: Mesh without adaptions (A) and close-up view around the biplane (B)

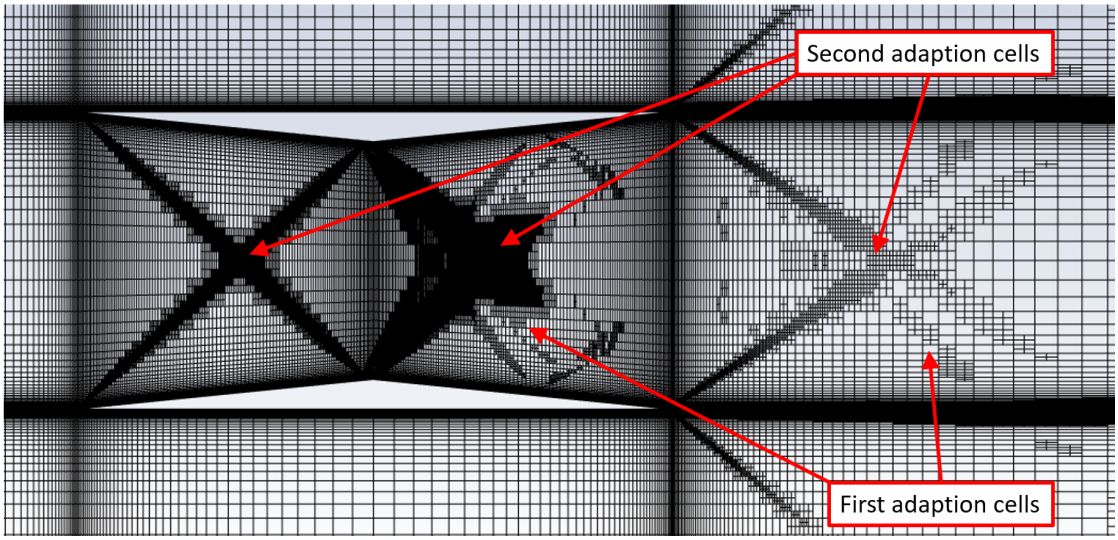

Figure 4: Two-step adaption of the mesh

After creating different adapted grids with increasing elements, a mesh independence study was performed to choose the mesh density that ensures mesh-independent solutions. This study aims to achieve a compromise between the accuracy of results and computational costs. To do so, the drag coefficient decomposition due to viscosity and pressure is analysed for three grid levels to confirm that the results are within the asymptotic range of convergence (NASA, 2021). According to Roache (1998), this asymptotic trend also indicates that the method is solved correctly. The GCI has been used to determine the meshes' discretisation error, considering the grid refinement ratio and the accuracy of the solutions. Even though the total GCI is small in the two steps, the medium mesh is chosen due to the small error between the medium and fine meshes and the more accurate results in terms of pressure drag compared to the coarse mesh. Discretisation error can also be derived from numerical diffusion, which is reduced using a structured mesh and a second order upwind method.

Table 1: Drag coefficients of the grid refinement study based on GCI (%) at design conditions

Mesh	Cells	y+	$C_{d,p}$	GCI	$C_{d,f}$	GCI	C_d	GCI
Coarse	256,833	0.93	0.00185	-	0.00796	-	0.00982	-
Medium	464,573	0.96	0.00179	4.467	0.00797	0.146	0.00976	0.725
Fine	770,245	1.07	0.00177	2.339	0.00796	0.237	0.00973	0.623

3.2.4 Simulation set-up

The main characteristics of the ”Setup” of the Outline View of Ansys Fluent 2022 R1 are explained hereunder. The software is initialised with double precision to avoid round-off errors (Gilkeson, 2023). Several processors working in parallel speed up the simulations by dividing the cases into different sections; they are solved separately and the information is finally shared. First, the general default settings have to be changed since density-based (or coupled) solvers usually obtain better solutions for high-speed compressible flows with shock waves due to the high-density variations across these discontinuities (ANSYS, 2022). Although pressure-based solvers used to be unable to solve compressible flows, this is no longer the case, so this kind of solver could have been chosen as well. Density-based solver simultaneously solves the governing equations of continuity, momentum, and energy, increasing the efficiency of the processing process (Gilkeson, 2023).

CFD software packages allow for the selection of multiple models for the simulation. Because of the presence of multiple shock waves, the energy equation must be turned on. Typically, CFD software employs RANS models to simulate the flow turbulence, which requires a proper turbulence model to be chosen (Cadence Design System, 2023). While other turbulence models employ wall functions to solve turbulent length scales in the boundary layer, the methods discussed hereunder require a finer mesh in the walls, although they obtain more accurate results (Gilkeson, 2022).

In this regard, most papers employ the SA turbulence model. This one-equation model is recommended because of its lower computational cost and accurate results for external flow with adverse pressure gradients, such as in this case. Nevertheless, some authors use k-ϵ and k-ω to simulate the Busemann biplane (Hosseini, 2019). The appropriate turbulence model may change depending on the applications of the study; therefore, a turbulence model sensitivity analysis has been carried out. Kusunose et al. (2011) investigation is used to compare the results and obtain an error. The conclusions, seen in Table 2, show that the lowest error is found for the SA method.

Table 2: Drag coefficients and error ($\%$) of the turbulence model sensitivity study

	Literature	Inviscid	ϵ	SA	ϵ	k-ϵ	ϵ	k-ω	ϵ
$C_{d,p}$	0.0019	0.0047	155.76	0.0018	3.17	0.0019	4.18	0.0024	28.02
$C_{d,f}$	0.0078	0.0000	100.00	0.0080	2.58	0.0075	3.23	0.0077	0.82
C_d	0.0096	0.0047	50.82	0.0098	1.47	0.0094	1.80	0.0101	4.73

Concerning the boundary conditions, they define the flow properties at the boundaries. In this case, three different boundary conditions have been used. As seen in Figure 2, the geometry is divided into an outlet formed by the right boundary of the domain, an inlet composed of the three other edges of the outer rectangle, and the walls of the biplane. The inlet is a pressure far-field, defining the free stream's velocity at infinity for compressible flows (ANSYS, 2013). However, this boundary requires the ideal-gas law to calculate the density and must be far enough from the object (10 c in this case). The gauge pressure is to be introduced; based on the ISA, its value is 101,325 Pa, which forces changing the operating pressure to zero (Cell Zone Conditions menu). Regarding the outlet, a pressure outlet with the same characteristics as the inlet is chosen in terms of gauge pressure and turbulence specification methods. The walls of the biplane are set as fixed walls, thus applying the no-slip condition that creates the boundary layer. Wall parameters are kept by default.

Finally, the solution methods are chosen according to the supersonic nature of the problem. The spatial discretisation scheme chosen is the Green-Gauss Node Based gradient, which is more accurate than the cell-based gradient at the expense of higher computational cost (ANSYS, 2015).

3.3 Convergence analysis

Along the project, the process of simulating a case has been explained. This section will describe the convergence criteria to avoid the convergence error that appears when the simulation is not correctly run. These criteria have been followed for every simulation carried out. When making the simulations, it is paramount to ensure that the numerical method reaches a solution (convergence); whether this solution is correct will be assessed in upcoming stages of the CFD workflow.

A given model may not converge because the finite volume method applied by CFD uses different algorithms and approximations to solve the Navier-Stokes equations. Hence, previous stages of the CFD pre-processing significantly influence convergence. Four main criteria have to be accomplished to affirm that a numerical solution has been achieved: the residuals being under an arbitrary threshold, the lift and drag variations being negligible in the later iterations, low mass and energy imbalances between the inlet and the outlet, and to have meaning physically; in other words, that the flow behaves naturally as expected from theory.

Residuals directly quantify the error in the solution of the governing equations. They measure the local imbalance of a conserved variable in each control volume. Since they represent a change in the properties of the flow between iterations, the residuals take variable times to converge and do not converge to the same numbers. In that sense, factors like starting the simulation from a good initialisation point help with the convergence of the residuals. It is more important that the residuals present a flat graph (stable residuals) rather than one in which the residuals are low if they are still changing. In this project, the convergence has been assumed if residuals stop varying after 10^{-3}, except for the energy residual, which had to reach a value of the order of 10^{-6} (ANSYS, 2015). In Figure 5, the shape of the residuals is seen. The two mesh adaptions are distinguishable by a sudden peak in the residuals. Other techniques used to facilitate the convergence of the case, such as starting the simulation with first order upwind in the spatial discretisation menu and then changing to the second, are also seen as discontinuities in the residual graph.

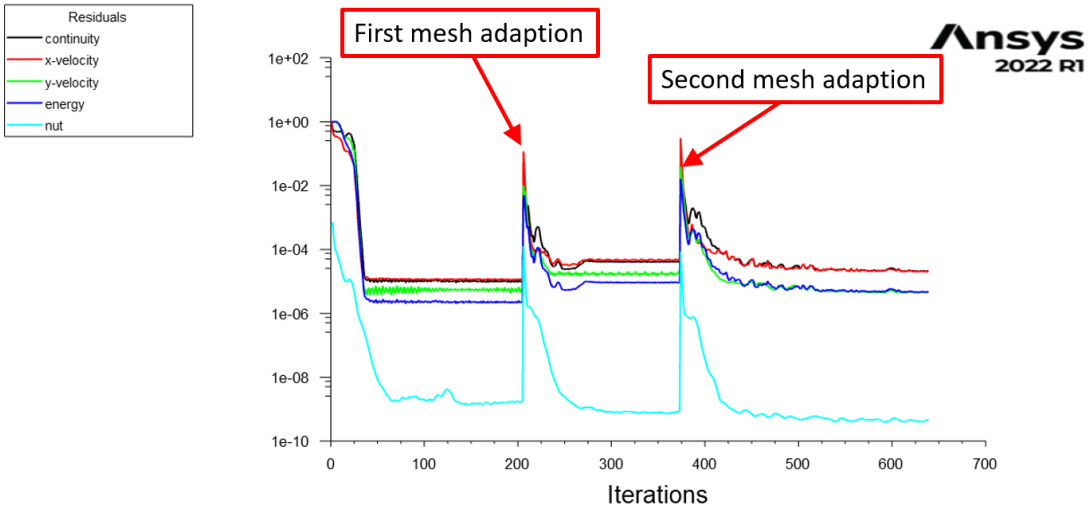

Figure 5: Residuals for design conditions of a Busemann biplane (Mach 1.7, 0 AoA)

Lift and drag variations are also monitored with respect to the number of iterations. These forces' reports usually oscillate for low iterations until the final value is approached, as seen in Figure 6. The convergence criterion is met when for a sensible number of the last iterations, for instance, a hundred iterations, variations of these forces are below 0.1%, similar to the case of the residuals.

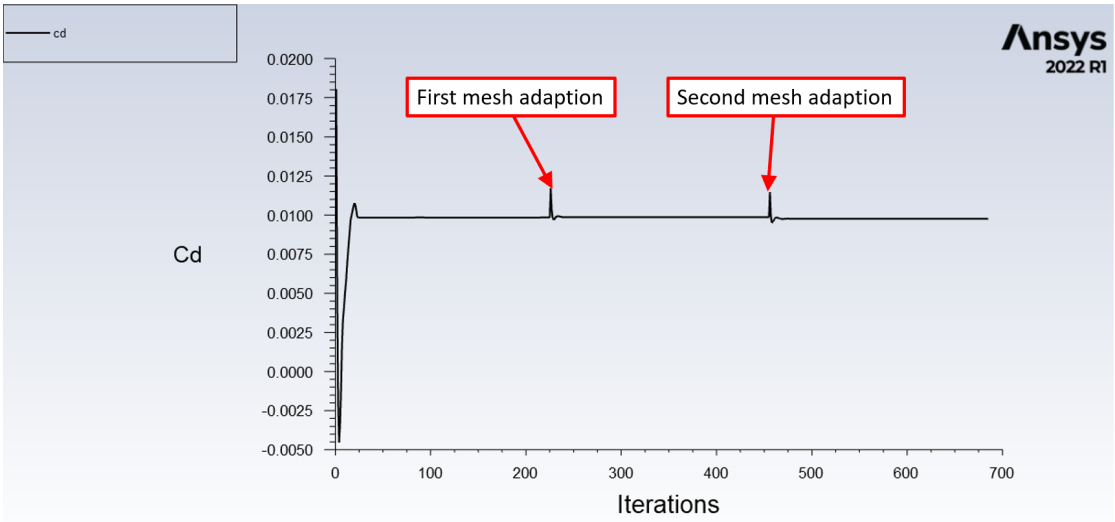

Figure 6: Drag coefficient report for convergence analysis

The imbalance of mass and energy is computed by subtracting the mass flow and energy recorded at the inlet and the outlet. This operation is expressed as a percentage and should be as close as possible to zero to achieve convergence. In this simulation, the imbalances approximate zero to the seventh decimal figure. Like in the case of the lift and drag variations, it can be monitored by a plot, although a report after the finalization of the simulation provides more accurate results.

Once the previous criteria have been checked, the simulation has likely converged. The last criterion consists of checking for anomalies in the flow's expected behaviour based on prior theoretical knowledge. Analysing the flow is also essential to see if there is any mistake in one of the earlier steps; for example, uniform flow next to the wall may indicate that the wrong boundary conditions are being used. Given the simulation's design conditions, the shock and expansion waves' location was checked.

3.4 Results and discussion

Once the results have been obtained, they must be analysed to get insight into the behaviour of the flow around the Busemann aerofoil. This is known as post-processing in CFD and permits understanding the key features of the flow. Nevertheless, as with any CFD simulation, the data must be verified and validated (V&V) since convergence does not imply reliable results (Oberkampf and Trucano, 2002). The verification process is based on accurately describing the physical model. The report has already justified solving the governing equations

with the correct mathematical tools.

On the other hand, validation refers to comparing the solution obtained and experimental or numerically accurate results. In this case, the numerical works of Kusunose et al. (2011) validate the results of the Busemann biplane in design conditions. The error was displayed in Table 2, where the SA model exhibits a maximum error of 3.17 $\%$ and a total error in the drag predictions of 1.47 $\%$. These errors may be caused by uncertainties in modelling the real flow physics or discretisation errors but are low enough to present an accurate description of the flow. Conversely, numerical results differ from the theory because of the presence of wave drag. Whereas theoretical analyses infer a complete cancellation of the wave drag at design conditions, numerical solutions account for the entropy generated by the non-linear expansion waves that increase the wave drag (Maruyama et al., 2011).

According to Gilkeson (2022), post-processing requires qualitative and quantitative methods to fully comprehend the flow. In this sense, qualitative methods propose a graphical alternative to study the general behaviour of the flow, which is particularly important in supersonic speeds to check the appearance of shock waves. For instance, Figure 10 presents a qualitative plot. In contrast, quantitative methods help compare the differences in the C_p and C_d among the different cases since they are not distinguishable to the naked eye.

Hence, Figure 7 displays a C_p plot across the symmetry axis of the biplane. The condition of equal pressure in the inlet and the outlet of the Busemann biplane, which was needed to reach design conditions, is verified. Furthermore, the increase in the pressure indicates the position of the shock waves, which is followed by another rise and the sudden decrease in pressure caused by Prandtl-Meyer expansion waves (NASA, 2021). Regarding velocity, its X-Y plot would be reversed since shock waves reduce the flow speed, contrarily to expansion waves.

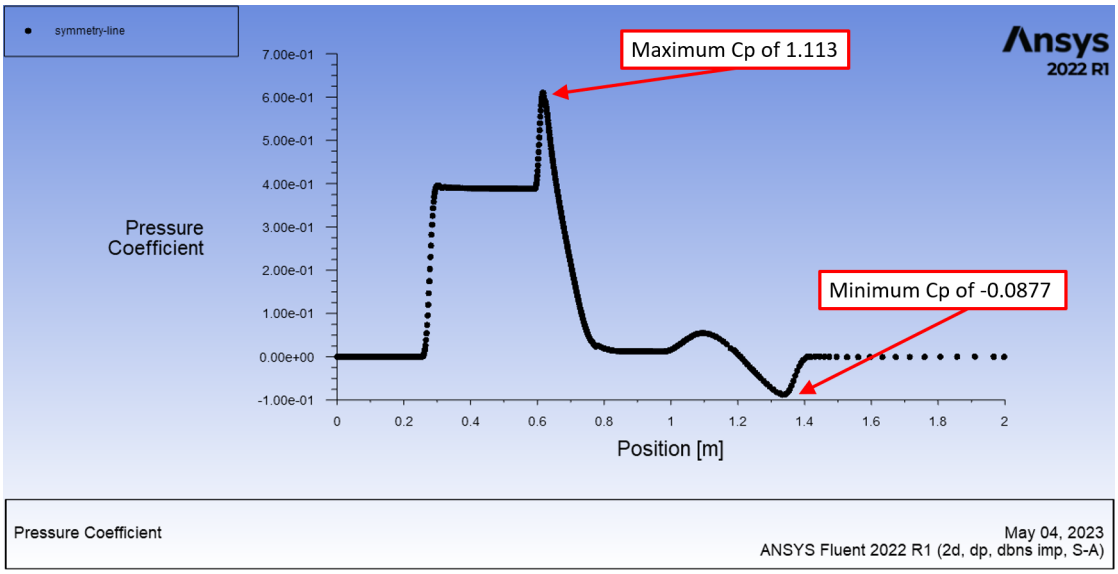

Figure 7: X-Y plot of the C_p along the symmetry axis of the Busemann biplane for design conditions

Focusing on flow characteristics, Figure 9 displays a contour plot of the C_p in which the aspects commented before can be seen. Shock and expansion waves are distinguished by a reduction and increase in pressure, respectively, caused by the decrease or increase of the area (NASA, 2021). Furthermore, a pressure peak arises in the inner wall of the biplane from an incomplete interaction between the shock and expansion waves (Maruyama et al., 2011). Thanks to the refinements of the mesh, these shocks are captured accurately. Observing the wave angles of the shock waves is important since they significantly impact the drag force. The no-slip condition besides the walls is also satisfied, as seen in Figure 9.

The same results can be obtained when analysing velocities. Figure 10 shows the velocity contour of the flow in the biplane, where the creation of expansion waves in the middle of the biplane accelerates the flow to the inlet conditions at Mach 1.7. Moreover, one conclusion that can be obtained from the streamlines seen in Figure 8 is that no recirculation is formed due to the high velocities of the flow and the sharp edges of the geometry. However, when increasing the angle of attack, recirculation may happen, introducing the appearance of detachment points that increase the drag of the

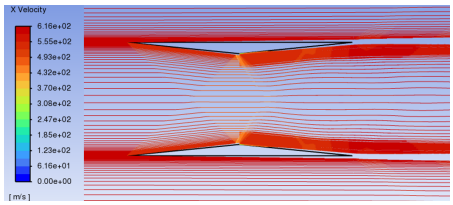

Figure 8: Streamlines passing through the biplane along with their X-velocity component

profile. Note that the streamlines only deviate slightly from their original direction when passing through the biplane.

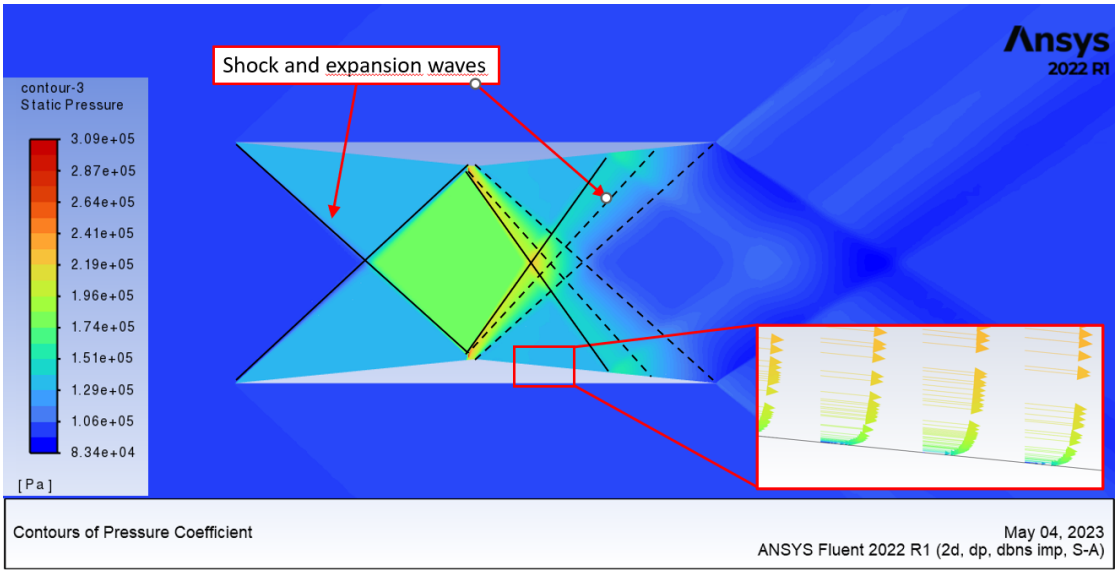

Figure 9: C_p contour plot around the biplane and capture of the main flow features

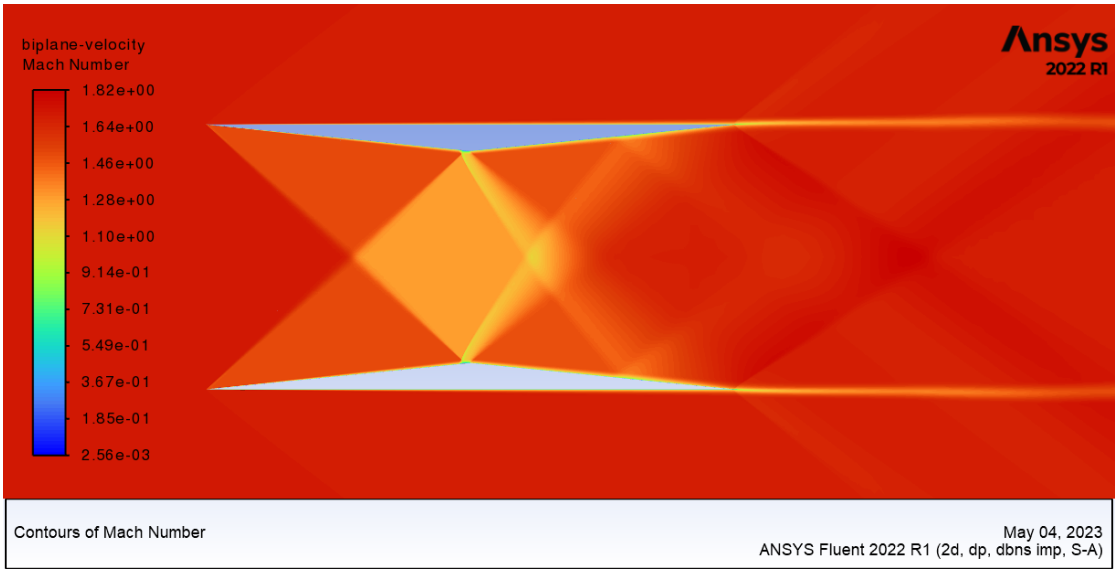

Figure 10: Velocity contour of the flow around the biplane in design conditions

4 Off-design Conditions Performance

4.1 Introduction

Design conditions have already been covered in the previous chapter. However, the minimisation of the drag entails zero lift generation due to the symmetry of the profile. For an aircraft that flies in cruise conditions, its weight is compensated by its lift, so the AoA has to be changed to increase the lift. Then, it can be concluded that design conditions may not appear in an actual flight, making the knowledge about the behaviour of the biplane in off-design conditions necessary.

In this section, off-design conditions are analysed. A parametric study of the velocity of the free stream and the angle of attack will be performed and synthesised. The data obtained with Ansys Fluent will be completed and compared with available literature resources to provide deeper insights into the properties of the supersonic biplane.

4.2 Mach number analysis

Two main intervals can be distinguished when talking about off-design Mach conditions of a Busemann biplane: before and after Mach 1.7. In this report, the speed range beyond the operation point is studied, although a discussion of speeds lower than Mach 1.7 provides insight into the challenges of incorporating a Busemann biplane in a real aircraft.

Studies by Patidar et al. (2016) indicate that the Busemann biplane suffers great losses in efficiency before Mach 1.7. The reason is the choking of the flow at low supersonic speeds, caused by the shape of the biplane, which is similar to a supersonic nozzle (Kusunose et al., 2011). This phenomenon creates a detachment of the shock wave, a curved shock wave that reduces the speed of the flow to a subsonic regime, which is accelerated to supersonic again after the expansions wave inside the biplane. The shock waves, as they are not generated inside the biplane, do not produce the wave-cancellation effect, increasing the wave drag of the aerofoil. This stops at Mach 1.7 due to the shock waves' attachment to the biplane's leading edges (Figure 9). This case was analysed in Section 3.

Greater Mach numbers between 1.7 and 2.1 have been analysed in CFD. The values of the drag coefficients are presented in Table 3 and compared with

Kusunose et al. (2011). The error is generally low, indicating the accuracy of the results, although it is far more important to analyse the trends of each aerodynamic coefficient. The pressure drag increases because of the shock pattern shown in Figure 12. On the contrary, the friction drag suffers a slight decrease that matches the theoretical assessment of this drag: when the airspeed is increased, the effects of viscous forces are less important, as seen in the rise of the Re. The overall drag grows when the Mach moves away from the design conditions. Nonetheless, the difference between off-design conditions and Mach 1.7 seen in Table 3 is not as notable as the discontinuity produced when decreasing the Mach number because the shock waves are still attached to the leading edges of the aerofoil.

The drag increase is a consequence of the asymmetry of the pressure distribution between the biplane, which, in turn, is translated into a reduction of the wave-cancellation effect (Patidar, 2016). A graphical evolution of the shock waves is shown in Figure 12. As commented before, the numerical calculations demonstrate that the increase in the Mach number results in the more significant overlapping of the shocks that escalates the wave drag.

Table 3: Drag coefficients for different stream velocities and error ($\%$)

Mach	$C_{d,p}$	$C_{d,f}$	C_d	ϵ
1.7	0.00179	0.00797	0.00976	1.47
1.8	0.00269	0.00773	0.0104	9.35
1.9	0.00618	0.00736	0.0135	1.29
2	0.00721	0.00727	0.0145	5.07
2.1	0.00913	0.00704	0.0162	5.56

Figure 12 presents a C_p X-Y plot in which the pressure coefficient is analysed in the symmetry plane of the aerofoil. As Mach increases, the angle of the shock wave decreases according to the expressions for oblique shock waves that relate flow variables upstream and downstream of the wave. This is seen in the delay of the first pressure peak. On the other hand, Prandtl-Meyer expansions are also delayed in the plot, indicating that they also present smaller wave angles. The change in the angle causes the asymmetry in the Busemann biplane, introducing wave drag, as explained before.

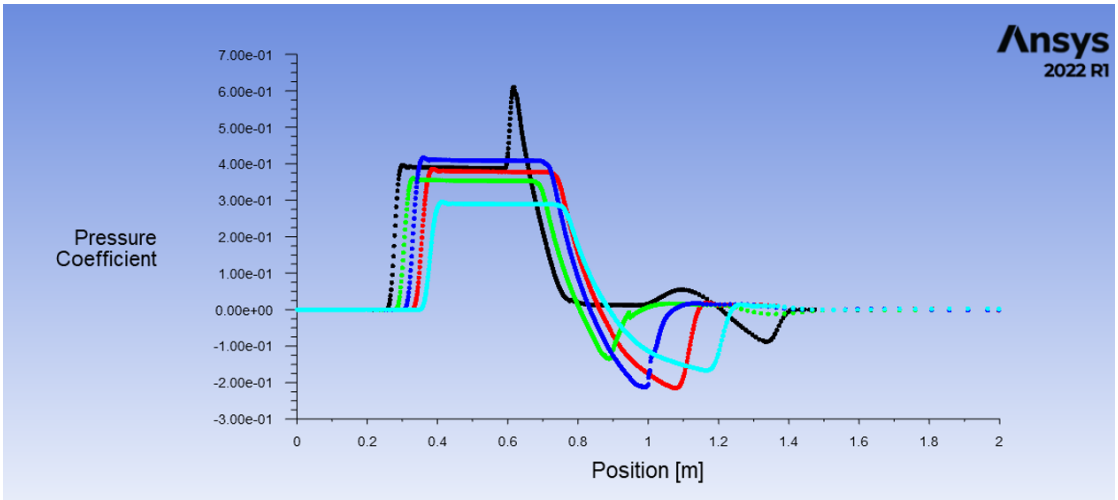

Figure 11: Comparison between the C_p along the symmetry axis of the biplane for Mach 1.7 (black), 1.8 (green), 1.9 (dark blue), 2.0 (red) and 2.1 (light blue)

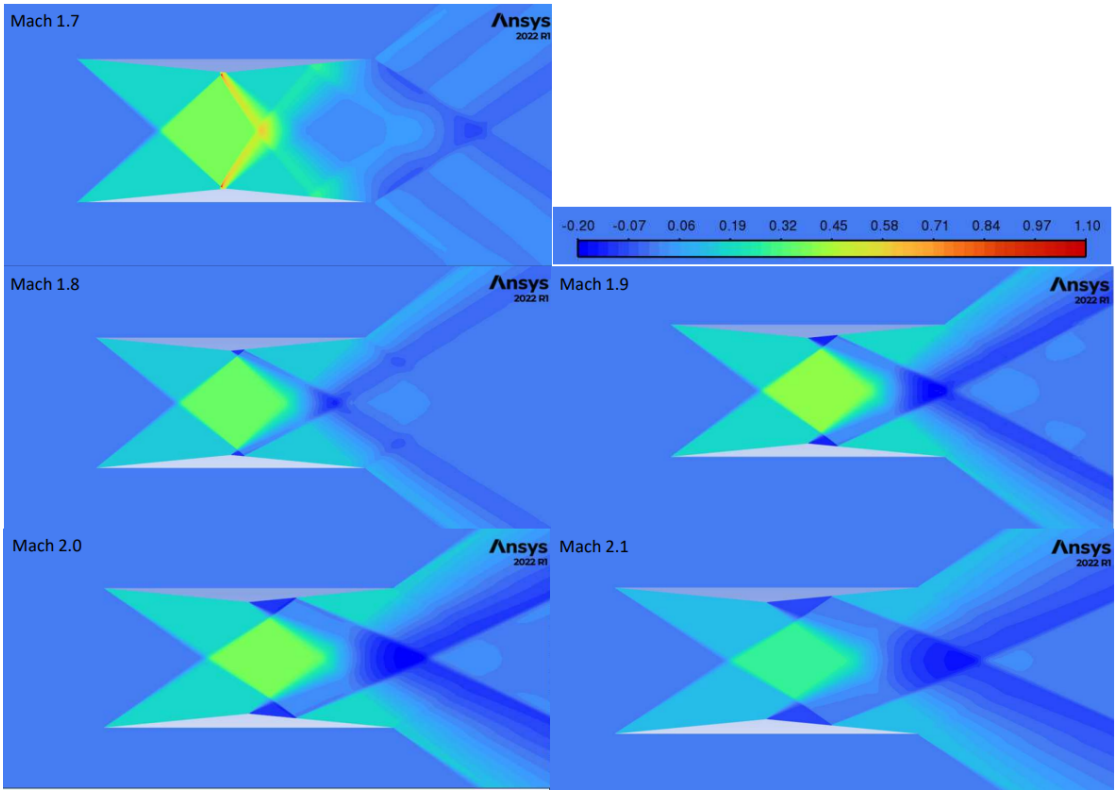

Figure 12: Shock-capturing C_p contour plot for different Mach numbers and zero AoA

4.3 Effect of changing the angle of attack

Separately from the analysis of the effect of Mach number on the behaviour of the flow, a parametric study of the AoA has also been carried out. By fix-

ing the Mach number to 1.7, the change in the AoA can be analysed without any interference from other parameters that may distort the conclusions. At the same time, this process saves computational costs since conclusions to changing the AoA and the Mach number can be inferred by combining the different consequences of each variable on the flow.

The study ranges from zero AoA to off-design conditions up to three degrees. The increase in the incidence of the free stream will increase the lift coefficient since the Busemann biplane is no longer symmetrical to the direction of the flow. Furthermore, the higher perpendicular area opposing the stream increases the lift and drag. Consequently, a larger wake can be inferred from the increase in drag. These simulations have to deal with areas of high turbulence (Figure 13) that are difficult to simulate with CFD. In fact, the flow detaches for high AoA near the middle section of the bottom part of the biplane. If high AoA are to be studied, the detachment of the flow may cause errors in the solutions. Therefore, the results of this section are also validated to ensure that they are accurate.

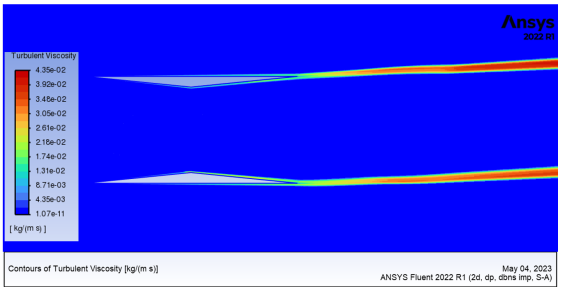

Figure 13: Turbulence viscosity of the boundary layer and the wake subjected to Mach 1.7 and AoA 3°

The lift presents a linear relation with respect to the AoA for low-incidence angles. Figure 14 presents the polar plot of the C_l within the range of study. The results were validated against the work of Kusunose et al. (2011), with a maximum error of 2.75 $\%$. Since the lift is generated by a pressure gradient between the intrados and the extrados of an aerofoil, Figure 15 illustrates the C_p contour plot for the different angles of incidence. Note that the higher the AoA, the higher the difference between the pressure coefficient of the external walls of the biplane.

In terms of drag, off-design conditions are created by the distortion in the wave angle of the shock and expansion waves. As in the previous section, this deviation of the shock pattern reduces the effects of wave drag cancellation. Still, the increase in the drag is compensated by a higher increase in the lift. Hence, the aerodynamic efficiency, defined as the ratio between lift and drag coefficients, is enhanced for the interval of AoA considered. These results match Patidar's studies on the effect of the AoA on the Busemann biplane.

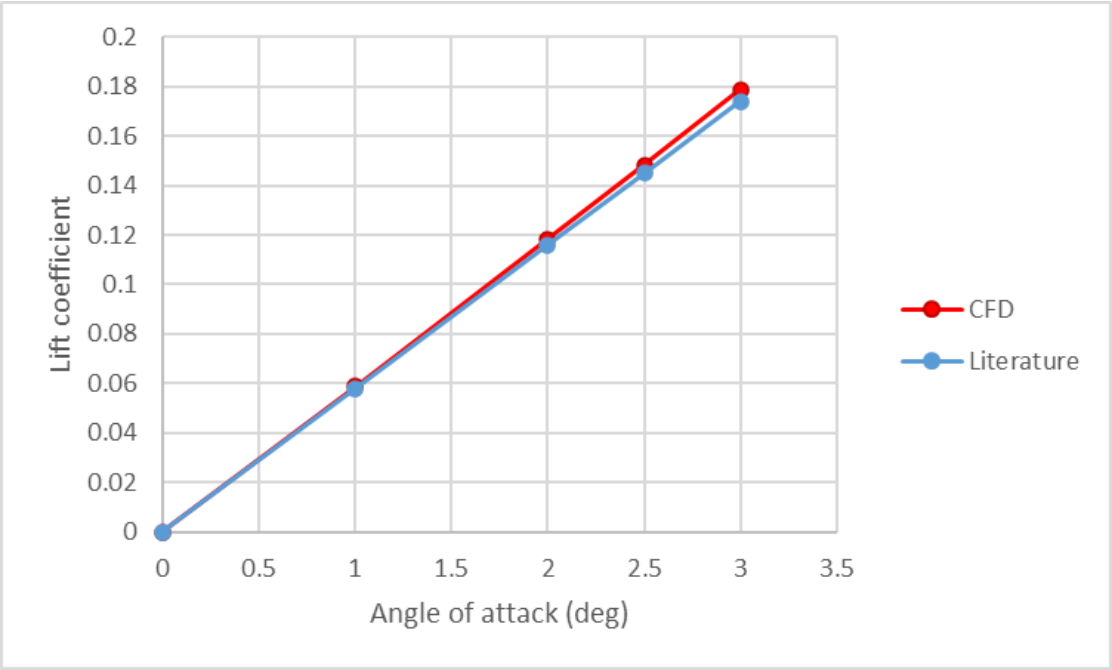

Figure 14: C_l vs AoA polar diagram for Mach 1.7

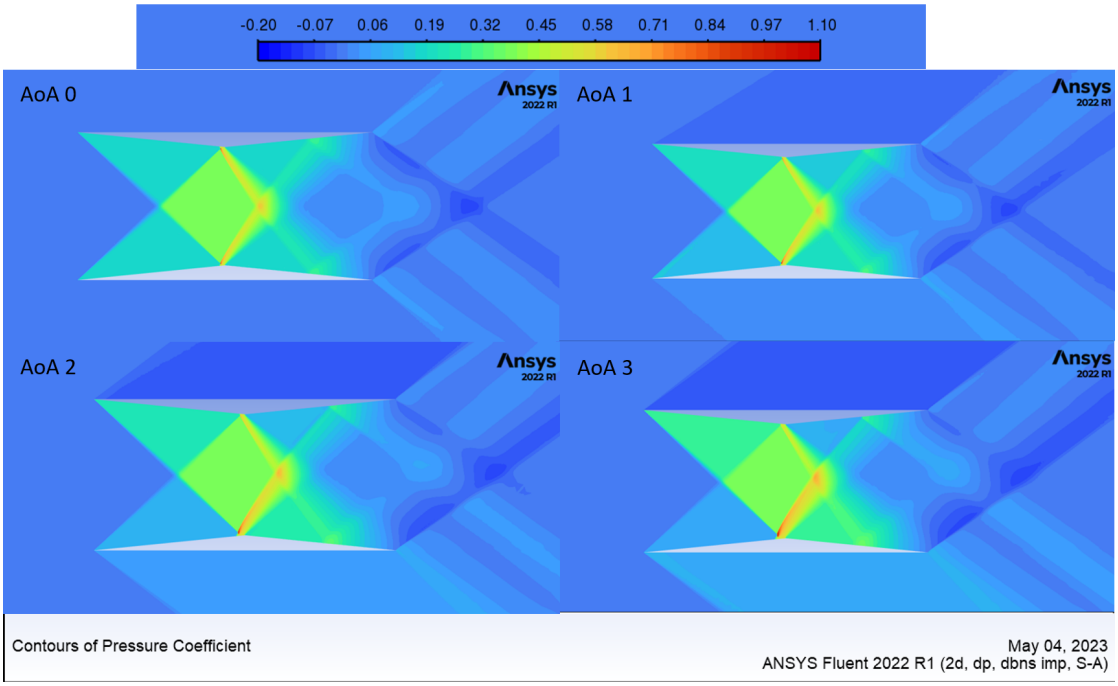

Figure 15: C_p distribution for different AoA and Mach 1.7

4.4 Implications in flight conditions

The two parametric studies were carried out to obtain a general understanding of the Busemann biplane for a given flight condition. Both results will be

combined and completed with the numerical analyses of Patidar et al. (2016), who simulated the biplane along with other supersonic aerofoils for a range of Mach numbers for each AoA considered in this report.

Summarising the results obtained above, the increase of the Mach number results in an increase of the total drag as a consequence of the reduction of the wave-cancellation effect. Since the analysis of the effect of airstream speed was performed at zero-lift conditions, the increase in drag is a net loss in terms of efficiency. However, these conclusions cannot be extrapolated to all AoA since the aerodynamic efficiency may increase if the lift makes up for the drag losses.

Regarding the study of the AoA, the change in the flow direction allows for calculating lift and drag coefficients. This information is more valuable concerning the actual behaviour of commercial aircraft since it establishes a relationship between fuel expenses and the cargo payload, the main reason behind supersonic transport's failure. Considering both results, the aerodynamic efficiency will be maximised by increasing the angle of attack, taking into account only the range of AoA studied in this report and overlooking the obvious stall complications that high AoA entail. For a given AoA, it can be concluded that increasing the velocity will negatively affect aerodynamic efficiency. Patidar's results validate these deductions, observing decreases in the efficiency of the Busemann biplane close to 40% when the Mach number is increased from design conditions to 2.5 for an AoA of 3°.

Having stated the conclusions, it must be added that this is not a practical solution for an actual aircraft. Perturbations during flight are common, making maintaining a constant speed challenging, especially in supersonic regimes. Hence, flying at design conditions would imply that a slight reduction of the aircraft's velocity is translated into the chocking of the wing and a sudden drag increase. While the report is focused on the Busemann biplane and these findings difficult the application of the aerofoil, the results constitute the starting point of new designs that reduce the problem mentioned.

5 Conclusion

5.1 Achievements

The aim of this project was successfully achieved, and each of the objectives was fulfilled. After selecting the geometry of the biplane, the project presents the CFD workflow that must be followed to perform the simulations, justifying every decision taken in the process. In that regard, the simulation setup and the meshing strategy were explained. Finally, the Busemann biplane was simulated and evaluated at a range of different off-design conditions to assess its viability in different flight conditions.

5.2 Discussion

As explained in Section 4, the key findings are related to applying a Busemann biplane in the wing of a supersonic aircraft. In that sense, Sections 3 and 4 concluded with the better performance of the aerofoil for maximum AoA and design velocity conditions. Although this idea is theoretically valid, its practical application would suffer from perturbations during flight. Even so, the Busemann biplane is the base of the wave-cancellation effect on supersonic aerofoils, and its understanding helps develop new designs.

Section 3 justified the numerical methods chosen to perform the simulations, which provided a firm foundation to have confidence in the results obtained. Even though the domain was not studied, the results were independent of its geometry, although a sensitivity study of the domain would have improved the computational efficiency. On the contrary, the sensitivity analysis of both the mesh and the turbulence model ensured the accuracy and fidelity of the results. In that regard, the maximum error found in the report is 9$\%$, an acceptable value considering that the average errors are around 1 to 5 $\%$.

However, the lack of experimental data about the Busemann biplane caused a biased selection of the turbulence model since the model used by the validating source was the same model (SA) that was finally chosen. This might be explained because the methods used for this model to solve the governing equations differ from the ones employed by other turbulence models, increasing the chances of obtaining larger errors. Even if the selection of the turbulence model significantly affected the accuracy of the results, the focus of this report is to obtain the correlations between the performance of the biplane and the inlet

parameters and not the accurate values for C_d and C_l.

While the simulations presented tend to converge with the proper refinements, the initial mesh selected in the mesh independence study (Section 3) could not perform a simulation for Mach numbers below 1.7. A possible cause may be the high-pressure gradients caused by the shock waves far away from the biplane, which cause divergence since the clustering of the cells was focused around the walls. Nevertheless, the information available in the literature (Kusunose et al., 2011, and Patidar et al., 2016) was used to complete the understanding of the biplane.

Even though the general behaviour of the biplane has been analysed, due to the complexity of these phenomena, choking and hysteresis were superficially covered. Studying these concepts in relation to the aerofoil behaviour is needed to provide a deeper insight into actual supersonic transport design.

5.3 Conclusion

This project was aimed at studying the performance of the biplane for different off-design conditions. The CFD workflow provided accurate results of the lift and drag coefficients of the biplane, demonstrated by their similarity to the validation data. Both parametric analyses were carried out under design conditions of the rest of the variables.

The results obtained for the Mach analysis show a clear detriment of the efficiency of the biplane as a result of the increase in wave drag. Although no simulations were performed at these speeds, it was found that the air resistance also increases for free stream velocities under design conditions. However, the discontinuities in the drag vs speed plot showed that, although is not optimal, increasing the velocity slightly affects the drag, while decreasing it below Mach 1.7 have drastic consequences in terms of drag.

On the contrary, the AoA increases the lift and even though the solutions also indicated a higher drag, the aerodynamic efficiency increases linearly with the AoA.

Although the real case of the Busemann biplane was simplified, it can be concluded that the results provide good insight into the functioning of the biplane.

5.4 Future Work

Many areas that were not covered may be proposed as future work. Investigating different proposed aerofoils and comparing them with the Busemann biplane may help to understand the current position of supersonic transport. In that sense, the report does not contemplate how the Busemann biplane would be able to reach design conditions from subsonic speeds without overcoming the drag. Furthermore, increasing the range of study of both the AoA and the Mach of the free flow can be interesting to better understand the flow physics in extreme conditions. For example, stall conditions may be simulated. Furthermore, the phenomena of choking and hysteresis can be specifically studied.

Finally, the 2D analysis could be extended into a 3D study of a wing. This enables the possibility of capturing the complex interactions in the real behaviour of the flow. The 3D analysis could include induced components of drag and how the lift and drag are distributed along the wing.

6 References

Anderson, D. J. 2003. Flight (Aerodynamics). In: Meyers, R. A. *Encyclopedia of Physical Science and Technology*. Third edition. New York: Academic Press.

ANSYS, I. 2013. ANSYS Fluent User's Guide. [Online]. Available from: http://www.pmt.usp.br/academic/martoran/notasmodelosgrad/ANSYS%20Fluent%20Users%20Guide.pdf

ANSYS, I. 2015. *ANSYS Fluent Theory Guide*. [Online]. Available from: http://www.pmt.usp.br/academic/martoran/notasmodelosgrad/ANSYS%20Fluent%20Theory%20Guide%2015.pdf

Bern, M. and Plassmann, P. 2000. Mesh Generation. In: J.-R. Sack and J. Urrutia. eds. *Handbook of Computational Geometry*. North-Holland, pp.291-332.

Busemann, A., 1935. Aerodynamic lift at supersonic speeds. Luftfahrtforschung, [e-journal] **12**(6), pp.210-220. Available from: https://www.mendeley.com/catalogue/aerodynamic-lift-supersonic-speeds/

Cadence Design Systems, I. 2023. *The Reynolds-Averaged Navier-Stokes (RANS) Equations and Models*. [Online]. Available from: https://resources.system-analysis.cadence.com/blog/msa2021-the-reynolds-averaged-navier-stokes-ra

Délery, J. M. 1999. Shock phenomena in high speed aerodynamics: still a source of significant concern. *The Aeronautical Journal*. Cambridge University Press, **103**(1019), pp. 19–34.

Emanuel, G. 2001. Shock Waves in Gases. In: Ben-Dor, G., Igra, O., and Elperin. T. Academic Press. *Handbook of Shock Waves*. ed. 2001. Academic Press. pp 185-262

Gilkeson, C. 2022. Lecture Slides. MECH5770M Computational Fluid Dynamics Analysis. School of Mechanical Engineering, University of Leeds.

Hosseini, E. 2019. CFD analysis of the aerodynamic characteristics of biconvex airfoil at compressible and high Mach numbers flow. *Springer*

Hu, R., Jameson, A., and Wang, Q. 2011. Adjoint based aerodynamic optimization of supersonic biplane airfoils. *Journal of Aircraft*. pp. 1-8.

Kusunose, K., Matsushima, K., and Maruyama, D. 2011. *Supersonic biplane—A review*. Progress in Aerospace Sciences. **47**, pp. 53-87.

Le, N., Shoja-Sani, A., and Roohi, E. 2015. Rarefied gas flow simulations of NACA 0012 airfoil and sharp 25–55-deg biconic subject to high order nonequilibrium boundary conditions in CFD. *Aerospace Science and Technology*. **41**. pp. 274-288.

Liu, J., Fan, X., Tao, Y., and Liu, W. 2019. Experimental and numerical study on the local unstart mechanism of hypersonic inlet. *Acta Astronautica*. **160**, pp 216-221.

Ma, B., Wang, G., Wu, J., and Ye, Z. 2020. Avoiding choked flow and flow hysteresis of Busemann biplane by stagger approach. *Journal of Aircraft*. **57**(3), 440-455.

Maruyama, D., Kusunose, K., Matsushima, K., and Nakahashi, K. 2011. Aerodynamic analysis and design of Busemann biplane: towards efficient supersonic flight. *Journal of Aerospace Engineering*. **226**(2), pp.217-238.

Matsushima, K., KUSUNOSE, K., Maruyama, D., and Matsuzawa, T. 2006. Numerical Design and Assessment of a Biplane as Future Supersonic Transport: Revisiting Busemann's Biplane. In:*25th International Congress of the Aeronautical Sciences*.

NASA. 2021. *CFD Analysis Process*. [Online]. Available from: `https://www.grc.nasa.gov/www/wind/valid/tutorial/process.html#geometrymodel`

NASA. 2021. *Examining Spatial (Grid) Convergence*. [Online]. Available from: `https://www.grc.nasa.gov/www/wind/valid/tutorial/spatconv.html`

NASA. 2021. *Expansion Fan Isentropic Flow*. [Ontline]. Available from: `https://www.grc.nasa.gov/www/k-12/airplane/expans.html`

NASA. 2021. *Oblique Shock Wave*. [Online]. Available from: `https://www.grc.nasa.gov/www/k-12/airplane/oblique.html`

NASA. 2021. *Prandtl-Meyer Angle*. [Online]. Available from: `https://www.grc.nasa.gov/www/k-12/airplane/pranmyer.html`

National Research Council. 1997. *U.S. Supersonic Commercial Aircraft: Assessing NASA's High Speed Research Program*. National Academy Press: Washington, DC.

Oberkampf, W.L. and Trucano, T.G.. 2002. Verification and validation in computational fluid dynamics. *Progress in Aerospace Sciences*. **38**(3), pp.209-272.

Patidar, V. K., Yadav, R., and Joshi, S. 2016. Numerical investigation of the effect of stagger on the aerodynamic characteristics of a Busemann biplane.

Aerospace Science and Technology. **55**, pp. 252-263.

Roache, P.J. 1998. Verification of Codes and Calculations. *American Institute of Aeronautics and Astronautics*. **36**(5), pp.696-702.

SimScale. 2022. Mesh Quality. *SimScale Documentation*. [Online]. Available from: https://www.simscale.com/docs/simulation-setup/meshing/mesh-quality/

Spalart, P.R. and Allmaras, S.R.A. 1992. One-equation turbulent model for aerodynamic flows. *AIAA 30th Aerospace Science Meeting and Exhibit*.

Yamashita, H., Yonezawa, M., Obayashi, S., and Kusunose, K. 2007. A Study of Busemann-Type Biplane for Avoiding Choked Flow. *American Institute of Aeronautics and Astronautics*.

Yamashita H., Kuratani N., Yonezawa M., Ogawa T., Nagai H., Asai K., and Obayashi S. 2013. Wind tunnel testing on start/unstart characteristics of finite supersonic biplane Wing. *International Journal of Aerospace Engineering*.

Zhai, J., Zhang, C., Wang, F., and Zhang, W. 2020. Design of a new supersonic biplane. *Acta Astronautica*. **175**, pp. 216-233.